

BAT: Better Audio Transformer Guided by Convex Gated Probing

Houtan Ghaffari^{*1} Lukas Rauch^{*2} Christoph Scholz^{2,3} Paul Devos¹

Abstract

Probing is widely adopted in computer vision to faithfully evaluate self-supervised learning (SSL) embeddings, as fine-tuning may misrepresent their inherent quality. In contrast, audio SSL models still rely on fine-tuning because simple probing fails to unlock their full potential and alters their rankings when competing for SOTA on AudioSet. Hence, a robust and efficient probing mechanism is required to guide the trajectory of audio SSL towards reliable and reproducible methods. We introduce *Convex Gated Probing* (CGP), a prototype-based method that drastically closes the gap between fine-tuning and probing in audio. CGP efficiently utilizes all frozen layers via a gating mechanism and exposes the location of latent task-relevant information. Guided by CGP, we rework the entire SSL pipeline of current SOTA audio models that use legacy implementations of prior SSL methods. By refining data preprocessing, model architecture, and pre-training recipe, we introduce *Better Audio Transformer* (BAT), and establish new SOTA on audio benchmarks.

1. Introduction

Self-supervised learning (SSL) has become the foundation of modern deep learning, generating state-of-the-art (SOTA) performance across modalities (He et al., 2022; Chen et al., 2020; Baevski et al., 2022a). In audio, progress has largely been achieved by adapting vision-based methods from images to spectrograms (Huang et al., 2022). While the AudioSet (Gemmeke et al., 2017) benchmark is repeatedly surpassed by novel SSL models (Chen et al., 2024; Alex et al., 2025), the evaluation methodology remains underdeveloped (Rauch et al., 2025a). Although benchmarks such as SUPERB (Yang et al., 2021) and HEAR (Turian et al.,

^{*}Equal contribution ¹Ghent University, Belgium ²University of Kassel, Germany ³Fraunhofer IEE, Germany. Correspondence to: Houtan Ghaffari <houtan.ghaffari@ugent.be>, Lukas Rauch <lukas.rauch@uni-kassel.de>.

Preprint. February 19, 2026.

2022) utilize frozen evaluation, the current pursuit of SOTA performance on AudioSet relies exclusively on fine-tuning. While fine-tuning may deliver the highest downstream performance, it introduces confounding variables (e.g., hyper-parameter sensitivity) that can obscure true progress (Kumar et al., 2022). As we show in this work, current SOTA results may reflect better optimization procedures rather than superior SSL representations. While frozen-feature probing has become an important evaluation technique in computer vision (Oquab et al., 2024; Darcret et al., 2025), simple probes fail to unlock the potential of audio embeddings, leading to a performance gap that falsely justifies reliance on fine-tuning (Rauch et al., 2025a). Reproducibility remains an additional challenge for recent SSL models in audio. For instance, EAT (Chen et al., 2024) and SSLAM (Alex et al., 2025) are built upon legacy code via fairseq (Ott et al., 2019) and inherit methodologies from Data2Vec 2.0 (Baevski et al., 2022a) and Audio-MAE (Huang et al., 2022). These implementations contain undocumented architectural details and unclear optimization practices, complicating reproducibility as we show in this work.

This work introduces *Convex Gated Probing* (CGP), a novel probing method designed for the faithful evaluation and efficient development of SSL models. Building on recent prototypical probing approaches (Rauch et al., 2025a), CGP employs a parameter-efficient gating mechanism to leverage the full depth of the frozen backbone, significantly closing the performance gap between frozen-feature probing and fine-tuning. Guided by CGP, we refine the audio SSL pipeline to propose the *Better Audio Transformer* (BAT). We systematically improve the data pipeline, target generation, and architecture. Our contributions are as follows:

Contributions

- Convex Gated Probing (CGP):** A novel SOTA probing protocol that enables faithful assessment without confounding factors of fine-tuning.
- Standardized methodology:** We identify inconsistencies in current audio SOTA pipelines (EAT, SSLAM) and establish a transparent and reproducible baseline.
- Better Audio Transformer (BAT):** We introduce BAT, a modernized SSL model that achieves SOTA performance on audio benchmarks.

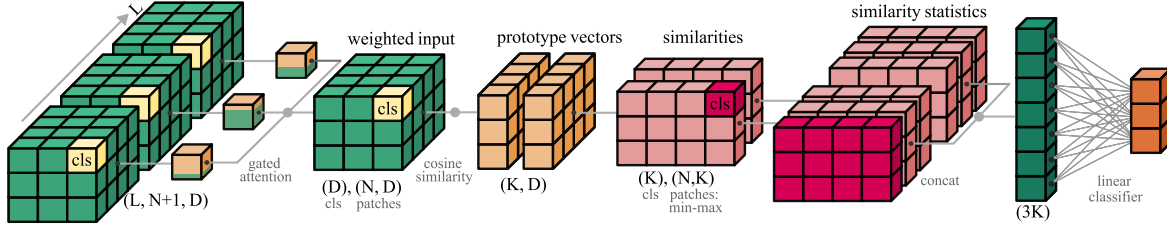


Figure 1. Convex Gated Probing (CGP). We illustrate the probing process of a spectrogram embedding for a ViT-Base backbone. CGP applies a learnable soft-gating vector (softmax) to compute a weighted sum of embeddings from all layers (L). The gating aggregates the hierarchy into a single representation, which is then compared against K prototypes. The cosine similarities of the patch embeddings are min-max pooled and concatenated with the ones from the `cls`-token, resulting in $3K$ features for a linear classifier.

2. Related Work

2.1. Probing

Evaluation with frozen embeddings. While benchmarks such as HEAR (Turian et al., 2022) use standardized probing protocols, the pursuit of SOTA performance on AudioSet (Gemmeke et al., 2017) relies predominantly on end-to-end fine-tuning (Rauch et al., 2025a). Although fine-tuning might maximize model performance, it can obscure the intrinsic quality of the representation by overwriting it (Kumar et al., 2022). Conversely, standard linear probes often underestimate embeddings, particularly in masked image modeling (MIM), since the semantic information is dispersed across token maps and layers rather than concentrated in the final `cls`-token (Przewięźlikowski et al., 2025; Alkin et al., 2025). While attentive pooling (Darcey et al., 2025; Psomas et al., 2025) improves an embedding’s summary, it forces a single-vector description. Recent work in audio shifts toward multi-vector aggregation. Niizumi et al. (2022) preserved the structure of patch tokens on the frequency axis by averaging the temporal axis of the embeddings, while prototypical probes (Rauch et al., 2025b;a) learn class-wise prototypes directly from the patch token map. By disentangling spatially dispersed events, prototypical probing shows that the large gap between frozen embeddings and fine-tuned models in audio is an artifact of the pooling method, positioning prototypical probing as a competitive alternative for SOTA evaluation.

Layer-aware evaluation. Previous works address the spatial bottleneck of the embeddings. However, extracting SSL embeddings from the last layer does not necessarily preserve intermediate information that may be better suited for a downstream task (Lee et al., 2023; Evcı et al., 2022). This is particularly evident in MIM architectures, where lightweight decoders might force the final encoder layers to assist in low-level reconstruction, causing semantic information to peak in middle layers (Alkin et al., 2025). Rauch et al. (2025b) confirms this geometric information shift, showing that the `cls`-token only becomes competitive with linear probes in audio after a supervised adaptation step that con-

centrates information in the final layer. Recent works in vision introduce alternative layer-aware strategies that utilize all available layers to adapt the model to a downstream task. Head2Toe (Evcı et al., 2022) first concatenates the embedding of all layers and employs a group lasso regularization to select the most informative ones, requiring a high memory cost during the feature selection phase. Side-Tuning (Zhang et al., 2020) trains a lightweight network in parallel, and sums its weights with the frozen backbone weights. More recently, Visual Query Tuning (VQT) (Tu et al., 2023) introduces learnable query tokens into the encoder to summarize intermediate features via attention, attempting to aggregate distributed semantics of a frozen backbone. Additionally, H2T-DFR (Hameed et al., 2024) combines Head2Toe with deep feature reweighting to combat spurious correlations.

Position of this paper for probing. Addressing these limitations, we propose CGB, a layer-aware probing method as a faithful alternative to exhaustive fine-tuning. Building on the binarized prototypes of Rauch et al. (2025b), CGB also resolves the hierarchical bottleneck by accessing the full depth of the backbone via a learnable soft-gating mechanism. Distinct from VQT (Tu et al., 2023) or Side-Tuning, CGB operates outside the architecture, avoiding internal modifications or attention bias. To prevent the dimensionality explosion typical of Head2Toe, we project layer features into compact prototype space *before* aggregation. Furthermore, by employing pooling (min, max) on prototype activations and utilizing the `cls`-token, CGB disentangles information across the model’s entire depth.

2.2. Self-Supervised Learning

Negative-Free Contrastive Learning. BYOL (Grill et al., 2025) represented a breakthrough in SSL by demonstrating that contrastive learning can succeed without negative pairs. It directly pushes the embeddings of two positive views closer together using a Siamese design (Bromley et al., 1993; Chen & He, 2020). Although this task admits trivial solutions, BYOL prevents this by: (i) incorporating the teacher-student framework (Buciluă et al., 2006; Tarvainen & Valpola, 2017; Hinton et al., 2015; Lillicrap et al., 2019;

He et al., 2020), where the teacher (target model) is the exponential moving average (EMA) of the student (online model), and (ii) using architectural asymmetry via a prediction head on top of the student. Although SimSiam (Chen & He, 2020) showed that EMA is not necessary to prevent trivial solutions in BYOL, it is an integral component in modern SSL approaches to achieve top results (Caron et al., 2021; Baevski et al., 2022a).

Masked Latent Regression (MLR). Baevski et al. (2022b) proposed Data2Vec (D2V) and extended BYOL to a structural MLR task across modalities, rather than learning modality-specific augmentation-invariant embeddings. Following MAE (He et al., 2022), which in turn was inspired by BERT (Devlin et al., 2019), it leverages a Vision Transformer (ViT) (Dosovitskiy et al., 2021) and applies intense masking for continuous data modalities. However, it does not drop the masked tokens from the encoder’s inputs and does not use a decoder (He et al., 2022) or architectural asymmetry (Grill et al., 2025). Masking dominates recent SSL algorithms in vision and audio, either as a prediction task (Zhou et al., 2022; Baevski et al., 2022b;a), or an augmentation (Assran et al., 2022). Hence, different masking strategies are explored, as they significantly affect the quality of the pretrained embedding. To our interest, D2V (Baevski et al., 2022b) used block-masking of BEiT (Bao et al., 2022) for the image modality, rather than random masking as in MAE (He et al., 2022). Masking has also been shown to be an effective data augmentation for clustering-based SSL (Zhou et al., 2022), even without explicit patch token prediction (Assran et al., 2022).

Collapse in MLR. Baevski et al. (2022b) notes that preventing collapse in MLR is challenging for continuous data due to the high correlation among neighboring tokens, particularly in audio. Although there are practical SSL algorithms based solely on whitening and feature diversity (Zbontar et al., 2021; Bardes et al., 2021; Ermolov et al., 2021), D2V (Baevski et al., 2022b) uses a hyperparameter-free approach that promotes variance by normalizing target representations across the sequence and feature dimensions. Interestingly, BYOL collapses without architectural asymmetry, but masked prediction and target normalization could prevent collapse in D2V. Additionally, Baevski et al. (2022b) demonstrated that averaging embeddings across multiple layers of the teacher produces better regression targets.

Improved MLR. Baevski et al. (2022a) proposed Data2Vec 2.0 (D2V2) by incorporating the efficiency technique from MAE (He et al., 2022) to avoid processing masked tokens in the encoder. They incorporated a lightweight CNN decoder into the student branch to predict the missing masked tokens in the latent space. For image modality, they found it beneficial to add a global loss using the `cls`-token (Peng et al., 2022) alongside the local loss for patch token prediction.

They also proposed inverse-block masking for better contextual representation learning. Additionally, they leveraged a multi-masking strategy (Assran et al., 2022) to reuse the target representations for multiple masked versions of the input in each forward pass.

Audio Self-Supervised Models. There are numerous audio SSL models, which are primarily extensions or direct applications of vision SSL models (Niizumi et al., 2021; Huang et al., 2022; Chen et al., 2024; Alex et al., 2025). SSAST (Gong et al., 2022) is an early work that introduced ViT (Dosovitskiy et al., 2021) to audio tasks. It combined masked spectrogram reconstruction and contrastive learning, although the latter was a reformulation of the former rather than a standard sample-wise contrastive learning (Chen et al., 2020). SSAST was introduced for audio prior to MAE (He et al., 2022) for images, but it did not have the efficiency of the MAE. Huang et al. (2022) propose Audio-MAE, an application of MAE to audio spectrograms, which are akin to grayscale images (albeit superficially in terms of 2D structure). Audio-MAE achieved top performance across six audio and speech classification tasks, including AudioSet, the primary benchmark for ranking audio SSL models. Following Audio-MAE, BEATs (Chen et al., 2023) introduce an iterative tokenizer to provide semantic targets for MIM, improving representation quality on AudioSet. Subsequently, Chen et al. (2024) propose EAT, a direct application of D2V2 (Baevski et al., 2022a) combined with the spectrogram data preprocessing of Audio-MAE, showing significant improvements on audio benchmarks. Finally, Alex et al. (2025) introduce SSLAM. It starts with pre-trained weights from EAT and applies the same algorithm in a second round of pre-training by adding an extra source retention loss to the objective. The source retention task is to predict unmixed targets from partially mixed samples in artificially mixed regions.

Position of this Paper for SSL. Per reports on AudioSet, SSLAM is the current SOTA model and surpasses EAT. Our investigation suggests that current SOTA results are not fully reproducible. We observed unclear implementation details, such as an extreme loss-scaling heuristic (e.g., factor of 8×10^4 for the global loss relative to the local loss). These two models rely on legacy implementations of D2V2 via fairseq (Ott et al., 2019) and Audio-MAE. We find that fine-tuning on AudioSet is sensitive to hyperparameter configurations, which complicates the reproduction of current SOTA results. To address these limitations, we systematically modernize the D2V2 framework to develop a better audio transformer, BAT. Guided by CGP, we integrate a dataset-independent preprocessing, gated-attention SSL targets, and increased decoder capacity, establishing a novel SOTA SSL model.

3. Audio Masked Latent Regression

We first explain the SSL algorithm from D2V2 (Baevski et al., 2022a), adopted by current SOTA audio models, EAT (Chen et al., 2024), and SSLAM (Alex et al., 2025).

Denote a ViT by f_θ , θ being the parameters that we optimize via gradient descent. We refer to this as the online model. We denote an EMA version of the model by $f_{\bar{\theta}}$, with $\bar{\theta}$ at batch step t updated via $\bar{\theta}^{(t)} = \lambda\bar{\theta}^{(t-1)} + (1 - \lambda)\theta^{(t)}$, i.e., after each batch gradient descent update of the online model. The decay rate, λ , is either fixed or modified via a linear scheduler. The $f_{\bar{\theta}}$ is the target model because it provides the SSL targets for the online model to bootstrap itself, i.e., self-distillation (Caron et al., 2021).

Denote an input audio spectrogram by $x_{spec} \in \mathbb{R}^{T \times F}$, T and F being the number of time and frequency bins, respectively. This input is organized into a sequence of flattened and non-overlapping $k \times k$ patches, denoted by $x \in \mathbb{R}^{N \times k^2}$, where $N = \frac{T}{k} \cdot \frac{F}{k}$. A significant portion of this input, about 80%, is randomly masked and removed to get a partial view $x_m \in \mathbb{R}^{n \times k^2}$. We denote the list of masked indices as \mathcal{I}_m .

The online model produces $(z_m, o_m) = f_\theta(x_m) \in \mathbb{R}^{n \times D} \times \mathbb{R}^D$, which are patch (z_m) and cls (o_m) tokens embeddings. During the SSL phase, the online model uses a CNN decoder to reconstruct missing patch tokens. Denote it by g_ϕ , and let $\tilde{z}_m = g_\phi(z_m) \in \mathbb{R}^{N \times D}$ be the online model prediction of the target patch embeddings. We denote the target model outputs by $(z, o) = f_{\bar{\theta}}(x) \in \mathbb{R}^{N \times D} \times \mathbb{R}^D$. Although the target and online encoders are identical, their forward passes differ. Let us expand the l -st ViT encoder block calculations,

$$z_a^{(l)} = MHSA(z_d^{(l-1)}), \quad (1)$$

$$z_b^{(l)} = LayerNorm(z_d^{(l-1)} + z_a^{(l)}), \quad (2)$$

$$z_c^{(l)} = MLP(z_b^{(l)}), \quad (3)$$

$$z_d^{(l)} = LayerNorm(z_b^{(l)} + z_c^{(l)}), \quad (4)$$

where $z_d^{(l)}$ is the output, including the `cls`-token. D2V (Baevski et al., 2022b) suggests multiple modifications to create targets, which D2V2 (Baevski et al., 2022a) inherits. First, the target network accumulates the patch embeddings $z_c^{(l)}$ from all layers into a list and drops the `cls`-tokens. Baevski et al. (2022b) find $z_a^{(l)}$ to be uninformative, and $z_c^{(l)}$ is a better target than $z_d^{(l)}$. These targets are standardized across the token axis (N). Then, the patch embeddings of all layers are averaged, followed by another standardization along the feature axis (D) to produce the target patch embeddings z . The normalizations are to prevent collapse and promote variance across tokens and embeddings. Additionally, the target network discards the `cls`-token embedding and uses $o = 1/N \sum_j z_j$. The

online model is optimized using this objective,

$$\underset{\theta, \phi}{\text{minimize}} \ell = \ell_{global} + \ell_{local}, \quad (5)$$

$$\ell_{global} = \|o - o_m\|_2^2, \quad (6)$$

$$\ell_{local} = \frac{1}{N} \sum_{i \in \mathcal{I}_m} \|z_i - \tilde{z}_{m_i}\|_2^2. \quad (7)$$

4. Convex Gated Probing

The primary motivation for CGP is that the best features of an SSL model may not reside in its final layer (Yang et al., 2021; Baevski et al., 2020). We illustrate the CGP method in Figure 1.

Denote a variant of an already pretrained ViT by f_θ^L , where $(z, o) = f_\theta^L(x) \in \mathbb{R}^{L \times N \times D} \times \mathbb{R}^{L \times D}$ indicate the patch and `cls`-tokens embeddings of a single input from all layers, with L the number of layers, N the number of patch tokens, and D the size of the embedding. CGP consists of K learnable prototype vectors, denoted by $P \in \mathbb{R}^{K \times D}$. The prototypes and the embeddings are first L2-normalized along the feature dimension,

$$\hat{P}_k = \frac{P_k}{\|P_k\|_2}, \quad \hat{z}_{ln} = \frac{z_{ln}}{\|z_{ln}\|_2}, \quad \hat{o}_l = \frac{o_l}{\|o_l\|_2}. \quad (8)$$

CGP has a learnable weight vector $a \in \mathbb{R}^L$ to aggregate the layers. It is first converted to convex weights via $\alpha = \text{softmax}(a)$, and then,

$$\bar{z} = \sum_l \alpha_l \hat{z}_l, \quad \bar{o} = \sum_l \alpha_l \hat{o}_l, \quad (9)$$

with $\bar{z} \in \mathbb{R}^{N \times D}$ and $\bar{o} \in \mathbb{R}^D$. The cosine similarities to prototypes are calculated as,

$$s_z = \bar{z} \hat{P}^\top, \quad s_o = \bar{o} \hat{P}^\top, \quad (10)$$

with $s_z \in [-1, 1]^{N \times K}$ and $s_o \in [-1, 1]^K$. The patch tokens' similarities, s_z , are summarized by taking their maximum and minimum across the tokens, and concatenated with the `cls`-token similarity,

$$s = [\min_N s_z, \max_N s_z, s_o], \quad (11)$$

resulting in $s \in \mathbb{R}^{3K}$, which is subsequently passed to a linear classifier. Table 1 presents the results of CGP, compared with fine-tuning and the previous best probing method, Protobin (Rauch et al., 2025a), on EAT and SSLAM, the current SOTA models on AudioSet. Crucially, our fine-tuning protocol precisely follows the reported procedure in their original works. Despite using the publicly available weights, we were unable to replicate the reported SOTA performance in fine-tuning, highlighting the sensitivity and

Table 1. Benchmark of EAT and SSLAM on AudioSet. Comparison between reported performance and our reproduction across fine-tuning and various probing settings (CGP, Protobin, LP).

Method	AS-20k		AS-2M	
	mAP	F1	mAP	F1
<i>Reported fine-tuning</i>				
EAT (Chen et al., 2024)	40.2	-	48.6	-
SSLAM (Alex et al., 2025)	40.9	-	50.2	-
<i>Our fine-tuning</i>				
EAT	40.28	30.73	47.61	36.63
SSLAM	39.97	27.03	47.69	36.83
<i>CGP Probing</i>				
EAT	35.20	26.04	41.04	19.51
SSLAM	34.62	24.58	40.20	19.59
<i>Protobin Probing</i>				
EAT	31.22	14.77	32.58	15.0
SSLAM	29.64	12.07	31.25	14.80
<i>Linear Probing</i>				
EAT	17.95	15.63	30.36	19.20
SSLAM	17.03	16.86	28.92	18.44

potential unreliability of fine-tuning. Consistent with findings by Rauch et al. (2025a), our evaluations (i.e., Protobin, CGP, and fine-tuning) show that SSLAM underperforms EAT. This suggests that reported improvements in these models may stem from optimization artifacts or dataset differences rather than the models’ embeddings. For Protobin and CGP, we use 10k prototypes. Figure 2 shows that this value provides a robust trade-off, as further increases in the number of prototypes yield diminishing performance gains.

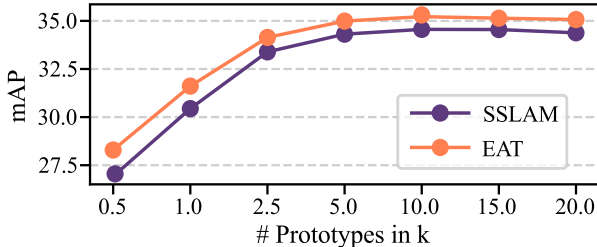


Figure 2. CGP Ablation. Increasing the number of prototypes constantly improves results, but yields diminishing returns. The best computation-performance trade-off is dataset-dependent.

5. Ablations for a Better Audio Transformer

The following ablation studies gradually introduce and evaluate the methodological enhancements in BAT.

Setup. All pre-trainings are conducted exclusively on AS-2M, containing 1,932,574 audio clips of 10 seconds each. The recordings are resampled to 16 kHz. Unlike EAT and SSLAM, we do not rely on the legacy fairseq

implementation of D2V2 (Baevski et al., 2022a) and Audio-MAE (Huang et al., 2022). We provide a new PyTorch implementation to foster reproducibility. For a fair comparison with EAT and SSLAM, we adopt similar hyperparameters across all pre-training experiments: batch size of 48 with 16 inverse-block masked views per sample, 400k optimization steps, 50k steps linear learning rate warmup from 1e-6 to 5e-4 and 350k steps cosine decay to 1e-6, and a weight decay of 0.05. In contrast to EAT and SSLAM, we exclude the large loss-scaling factors inherited from the D2V2 framework. We found that scaling the global token loss by 8×10^4 creates optimization instability and compromises reproducibility, as evidenced by our initial findings. By weighting global and local losses equally, we maintain a simplified and transparent objective that avoids the need for heuristic scaling. We also use bfloat16 mixed-precision optimization instead of float16. All ablations are conducted on AS-20k utilizing CGP with 10k prototypes. A detailed overview of hyperparameters is available in Appendix A.

5.1. Better Data Preprocessing Pipeline

Conventional audio frontends utilize a spectrogram generation, dynamic range compression, and normalization to prepare the input signal. As shown by Ghaffari & Devos (2024), frontend choices are critical to performance, influencing feature details, noise sensitivity, and the efficiency of gradient-based optimization. EAT and SSLAM adopt log-compressed mel-spectrogram (filterbanks) and global standardization of Audio-MAE. This pipeline relies on a legacy implementation that concentrates on human speech. Furthermore, the use of global normalization complicates the practical deployment of pre-trained models, as it requires knowledge of dataset statistics for downstream tasks.

Table 2. Input processing ablation. We compare different spectrogram representations and normalization strategies. The **baseline** denotes our reproduction of the filterbank inputs used in EAT and AudioMAE, while our **BAT** configuration is highlighted.

Data Pipeline	Global Statistics	mAP	F1
EAT (reproduced)	✓	34.86	24.28
Ours	✗	35.03	24.75

We extract mel-spectrograms using a modern TorchAudio implementation that avoids heuristic filtering and supports efficient batch transformations, ensuring better signal integrity and training speed. We then apply a decibel-scale log-compression to improve dynamic range relative to a bare log function. Finally, we apply local min-max normalization to scale each mel-spectrogram to $[0, 1]$, thereby suppressing noise effectively and facilitating easier deployment (Ghaffari & Devos, 2024; 2025). Results in Table 2 indicate that our pipeline enhances model performance while remaining independent of dataset statistics, ensuring a more robust and

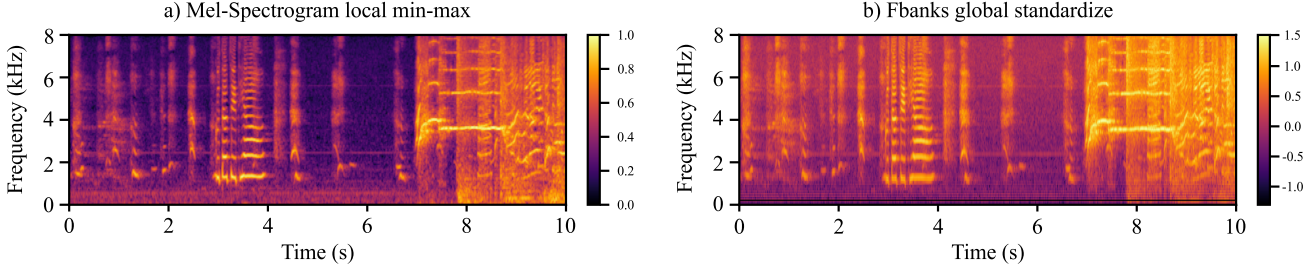


Figure 3. Impact of audio frontend. A recording containing the labels [Whimper, Gasp, Speech, Outside, urban or manmade]. (a) Our incorporated audio frontend: Mel-spectrogram with decibel compression and local min-max normalization, exhibiting clear spectral structure and high contrast. (b) Audio-MAE, EAT, and SSLAM: simple log, filtering, Mel-spectrogram, and global standardization. Note the artifacts and blurring, particularly at lower frequencies.

flexible solution than legacy implementations. Figure 3 provides a visual comparison of the mel-spectrograms produced by the legacy and our frontends.

5.2. Better Targets with Gated Attention

Table 3. Impact of target selection and attention gates. EOB denotes End-of-Block. The baseline from the previous section and our proposed **BAT** configuration are highlighted.

SSL Target	Gated Attention	mAP	F1
MLP	✗	35.03	24.75
EOB	✗	34.60	25.00
MLP	✓	35.09	26.12
EOB	✓	35.42	27.13

D2V (Baevski et al., 2022b) generates targets by averaging the outputs of the MLP across multiple teacher layers (see Section 3). This design choice emerges from an empirical investigation that shows that using MHSA output as a target led to representation collapse. Notably, using the End-Of-Block (EOB) output, which sums the MLP and MHSA modules, yields inferior results to MLP. Although their solution improved the results, it violates the semantics of the encoder block as a coherent function. We hypothesize that the performance degradation observed with EOB targets stems directly from the MHSA component, which introduces noisy inter-token dependencies into the residual connection (e.g., attention sinks), corrupting the semantic quality of the targets. Recent findings in LLMs (Qiu et al., 2025) demonstrated that applying a sigmoid gate after the attention-weighted value projection improves performance, scaling properties, and training stability. Qiu et al. (2025) identified two factors contributing to the effectiveness of attention gating in MHSA: (i) introducing non-linearity between value and output projections in the attention block, and (ii) introducing input-dependent sparsity to attention scores, which eliminates attention sinks (Xiao et al., 2024) and enhances long-context extrapolation performance. We propose incorporating this gating mechanism (Qiu et al., 2025) to improve attention and utilizing the EOB output as

the SSL target.

We denote the input to MHSA as $x \in \mathbb{R}^{N \times D}$. MHSA applies three linear projections to produce queries, $Q = xW_Q$, keys, $K = xW_K$, and values $V = xW_V$. To accommodate multi-head processing with H heads, these are reshaped and transposed as $\mathbb{R}^{N \times D} \rightarrow \mathbb{R}^{H \times N \times d_h}$, where $d_h = D/H$. The attention-weighted values are,

$$\bar{V} = \text{softmax}\left(\frac{QK^\top}{\sqrt{d_h}}\right)V, \quad (12)$$

where $\bar{V} \in \mathbb{R}^{N \times D}$ after transposing and reshaping the results of the above equation (implicitly vectorized on the head axis). The default MHSA applies a final linear projection to produce $O = \bar{V}W_O$. However, the gating mechanism, which we adopt, is as follows,

$$\tilde{V} = \sigma(xW_G) \cdot \bar{V}, \quad (13)$$

$$O = \tilde{V}W_O, \quad (14)$$

where $W_G \in \mathbb{R}^{D \times D}$ and the gate results after the sigmoid activation, $\sigma(\cdot)$, is multiplied element-wise with attention-weighted values.

Table 3 presents the ablation of target selection and attention gating. Consistent with prior literature (Baevski et al., 2022b), utilizing EOB targets without gating degrades model performance compared to the MLP baseline. However, integrating the gated attention mechanisms reverses this observation. Gating not only improves the baseline but also unlocks the potential of the EOB targets, resulting in the highest performance. This supports our hypothesis that the gating mechanism mitigates the inherent limitations of the MHSA in this SSL dynamic. Figure 5 shows the positive effect of gating on attention maps.

5.3. Better Decoder for a Better Encoder

D2V2 (Baevski et al., 2022a) uses a lightweight CNN decoder. However, He et al. (2022) show that a sufficiently large decoder improves the encoder performance on downstream tasks. If the decoder is weak, the later layers of the

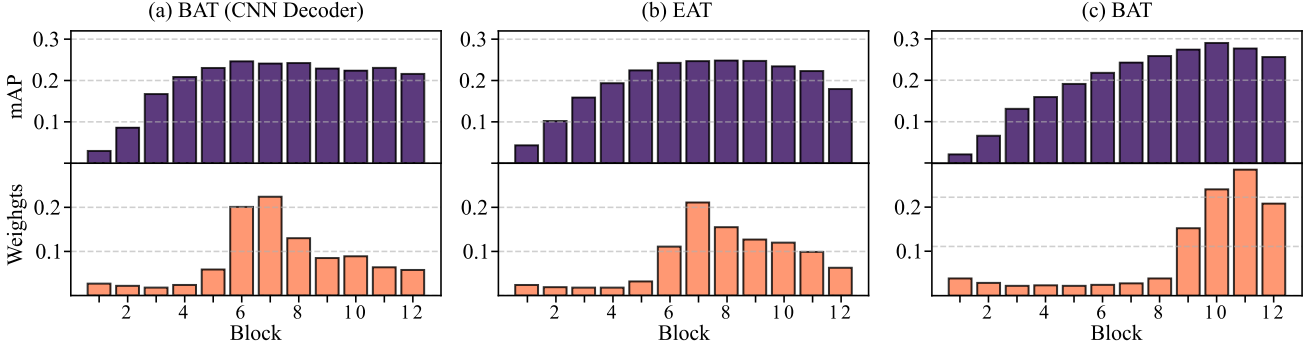


Figure 4. Layer-wise latent information. We display the layer-wise latent information quality across three models on AS-20k: (a) BAT with the lightweight CNN (best performer from Table 3), (b) EAT (baseline), and (c) our final BAT (ViT decoder). The top row displays the linear probing performance of each Transformer block. The bottom row visualizes the learned gating weights from CGP. Notably, the standard EAT (b) and the CNN-based BAT (a) exhibit a middle-heavy distribution where semantic information peaks early. In contrast, the heavy ViT decoder in the final BAT (c) shifts the semantic peak toward the later layers, improving linear separability at the output.

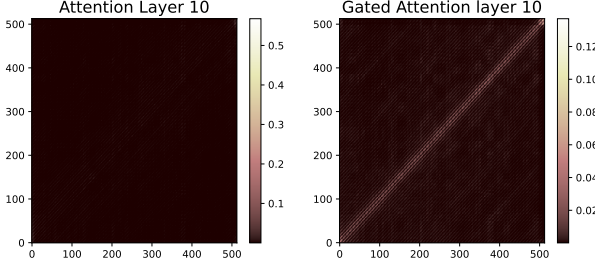


Figure 5. Impact of gating on attentions. Gating distributes the attention better and focuses more on the token itself, rather than sinking into one token, primarily the `cls`-token.

encoder should contribute more to masked token reconstruction rather than to learning high-level semantics (Huang et al., 2022), thereby diminishing the model’s effective capacity. This is particularly pronounced in regression-based MIM (Alkin et al., 2025), affecting the quality of frozen-feature probing. We replace the six-layer CNN decoder with a six-layer ViT decoder and examine how varying the number of heads and the MLP ratio affect encoder performance.

Table 4 shows that replacing the CNN with a more expressive ViT decoder yields a substantial performance improvement of 2.0 percentage points (pp) in mAP. Further increasing the decoder capacity yields 37.52 mAP, a modest improvement over the reproduced EAT baseline of 34.86 mAP in Table 2. Additionally, we utilize CGP to analyze the layer-wise distribution of latent information within the frozen encoder. Figure 4 illustrates this relationship by displaying both the per-block linear probing performance and the learned gating weights of CGP. We observe a strong correlation between these two metrics, suggesting that CGP can automatically identify the most informative layers without the need for exhaustive manual probing of each individual block. Comparing the architectures shows that the CNN-based BAT with attention gates (best performing model

from Table 3) (a) and the standard EAT baseline (b) exhibit a centered distribution, where semantic quality peaks around block 7 and degrades in the final layers. This suggests that the lightweight decoder forces the encoder’s deeper layers to retain low-level reconstruction details. In contrast, our final BAT with a ViT decoder (c) shifts the semantic peak significantly to the right (blocks 10-12). This architectural shift not only improves the final representation but also boosts per-block utility: BAT achieves a peak linear probing accuracy of nearly 30 mAP in the final block, whereas the baseline models struggle to surpass 25 mAP at any depth. This demonstrates that BAT produces richer embeddings that are more linearly separable, making it highly practical for downstream tasks.

Table 4. Impact of decoder. We replace the lightweight CNN decoder with a ViT. The baseline from the previous section and our proposed BAT configuration are highlighted.

Decoder	Depth	Heads	MLP Ratio	mAP	F1
CNN	-	-	-	35.42	27.13
ViT	6	6	2	37.43	28.91
ViT	6	12	4	37.52	29.11

6. Benchmark Results

This section introduces the main benchmark results of our BAT model. We summarize the results in Table 5.

Setup. Following established protocols for AudioSet benchmarks, we validate our method across four standard datasets: AS-20k, AS-2M, ESC-50 (Piczak, 2015), and Speech Commands V2 (SC-2) (Warden, 2018). More details are available in Appendix C. We evaluate the current SOTA baselines (EAT and SSLAM) by replicating their fine-tuning recipes within our framework. For evaluating BAT, we adopt their hyperparameters for fine-tuning without further optimization. Additionally, we report frozen results using linear

Table 5. Downstream task performance comparison across audio and speech benchmarks. We evaluate models using fine-tuning (FT), our convex gated probing (CGP), and linear probing (LP). BAT consistently outperforms EAT and SSLAM baselines, showing substantial gains in the frozen embedding setting.

Model	# Params	Data	AS-2M			AS-20K			ESC-50			SC-2		
			FT	CGP	LP									
<i>Reported</i>														
EAT	88M	AS-2M	48.6	-	-	40.2	-	-	95.9	-	-	98.3	-	-
SSLAM	88M	AS-2M	50.2	-	-	40.9	-	-	96.2	-	-	98.1	-	-
<i>Our tuning/probing</i>														
EAT	88M	AS-2M	47.61	41.04	30.36	40.28	35.20	17.95	95.45	94.05	81.30	97.88	95.57	72.68
SSLAM	88M	AS-2M	47.69	40.18	28.92	39.97	34.62	17.03	94.80	94.70	88.00	97.87	95.53	53.51
BAT	91M	AS-2M	48.55	42.90	34.27	41.32	37.52	25.59	95.52	95.80	87.25	98.13	97.13	72.83

probing and our CGP. Comprehensive hyperparameter details for all protocols are provided in [Appendix A](#).

Frozen-feature probing. BAT consistently outperforms the current SOTA baselines in the frozen-feature setting by a substantial margin across all evaluated benchmarks. The superiority is most evident in the complex AS-2M and AS-20k tasks, where BAT’s linear and CGP performance significantly exceeds that of EAT and SSLAM. In particular, the linear probing results suggest that the final block’s embeddings from BAT contain more viable information. Furthermore, our results highlight the utility of our robust CGP in bridging the gap with fine-tuning. For instance, on AS-20K, CGP performance is within 3.8 pp mAP of our new fine-tuning SOTA. On ESC-50, BAT with CGP even outperforms fine-tuning. These results highlight the challenges of using fine-tuning for model assessment, whereas CGP yields more robust insights by isolating the frozen representations from the stochasticity of the fine-tuning process.

Reproducibility and fine-tuning. We observe a notable discrepancy between performance reported in the literature and our reproductions, particularly regarding SSLAM. Except for AS-2M finetuning, EAT results were largely reproducible, although we also could not reproduce their pre-trained SSL model with their exact recipe (see [Table 2](#)). In comparison, the 40.9 mAP reported for SSLAM on AS-20k was not reproducible using the provided hyperparameter settings. Under this standardized condition with the legacy hyperparameters, BAT consistently outperforms our reproduced baselines for EAT and SSLAM. We attribute this to our SSL improvements guided by CGP. While BAT does not reach the peak reported figures of prior works, we emphasize that our results were achieved without any dataset-specific hyperparameter tuning. We anticipate that such optimizations would further extend the performance gap between BAT and existing SOTA models. As shown in [Figure 4](#), the location of task-relevant latent information shifts significantly in our model compared to baselines.

Task-relevant latent information. As illustrated in [Figure 4](#), a major factor for the superiority of BAT is an increase in the utilized capacity of the encoder by offloading the reconstruction task to an expressive decoder. However, we caution against overgeneralizing “later-is-better” as a universal metric. Different architectures or SSL objectives may yield underutilized encoders that peak in the middle layers while maintaining competitive performance. Therefore, the semantic shift observed in BAT is only a sign of better embeddings in this model.

7. Conclusion

In this work, we revisited the evaluation practices of audio Self-Supervised Learning (SSL). We demonstrated that the reliance on fine-tuning when competing for SOTA on AudioSet makes it difficult to fairly evaluate and reproduce the models. To address this, we proposed the prototype-based Convex Gated Probing (CGP). By efficiently aggregating features across all layers, CGP drastically closes the performance gap between frozen evaluation and fine-tuning, outperforming the prior SOTA probing method, Protopin. Guided by CGP, we introduced the Better Audio Transformer (BAT), a fully modernized implementation of the masked latent regression for audio SSL. We incorporated a gating mechanism for attention, which not only improved the model overall but also yielded better targets for SSL. BAT establishes new SOTA results on audio benchmarks, while ensuring reproducibility. We release the code upon acceptance or request during the review process. In future work, we will evaluate the generalization of BAT and CGP in specialized domains such as bioacoustics (e.g., BEANs ([Hagiwara et al., 2023](#)) or BirdSet ([Rauch et al., 2025c](#))) to further benchmark its performance in comparison with domain-specific models such as Bird-MAE ([Rauch et al., 2025b](#)). Additionally, we aim to investigate BAT scales across both model and data dimensions by evaluating larger parameter counts and more diverse audio corpora.

Impact Statement

This work advances the field of self-supervised audio representation learning. By improving the effective depth of encoders and introducing efficient probing methods like CGP, we contribute to more resource-efficient model evaluation. This has potential positive societal impacts by reducing the computational overhead and carbon footprint associated with developing state-of-the-art audio models. Furthermore, improving the robustness of frozen embeddings might improve the accessibility of high-performance models for researchers with limited compute resources. We do not see any specific negative ethical consequences unique to this work.

References

- Alex, T., Ahmed, S., Mustafa, A., Awais, M., and Jackson, P. J. SSLAM: Enhancing Self-Supervised Models With Audio Mixtures For Polyphonic Soundscapes. In *International Conference on Learning Representations (ICLR)*, 2025.
- Alkin, B., Miklautz, L., Hochreiter, S., and Brandstetter, J. Mim-refiner: A contrastive learning boost from intermediate pre-trained representations. In *International Conference on Learning Representations (ICLR)*, 2025.
- Assran, M., Caron, M., Misra, I., Bojanowski, P., Bordes, F., Vincent, P., Joulin, A., Rabbat, M., and Ballas, N. Masked siamese networks for label-efficient learning. In *European Conference on Computer Vision (ECCV)*, 2022.
- Baevski, A., Zhou, H., Mohamed, A., and Auli, M. Wav2vec 2.0: A framework for self-supervised learning of speech representations. *Advances in Neural Information Processing Systems (NeurIPS)*, 2020.
- Baevski, A., Hsu, W.-N., Xu, Q., Babu, A., Gu, J., and Auli, M. data2vec: A general framework for self-supervised learning in speech, vision and language. In *International Conference on Machine Learning (ICML)*, 2022a.
- Baevski, A., Hsu, W.-N., Xu, Q., Babu, A., Gu, J., and Auli, M. data2vec: A general framework for self-supervised learning in speech, vision and language. In *International Conference on Machine Learning (ICML)*, 2022b.
- Bao, H., Dong, L., Piao, S., and Wei, F. Beit: Bert pre-training of image transformers. In *International Conference on Learning Representations (ICLR)*, 2022.
- Bardes, A., Ponce, J., and LeCun, Y. Vicreg: Variance-invariance-covariance regularization for self-supervised learning. *arXiv preprint arXiv:2105.04906*, 2021.
- Bromley, J., Guyon, I., LeCun, Y., Säckinger, E., and Shah, R. Signature verification using a "siamese" time delay neural network. In *Advances in Neural Information Processing Systems (NeurIPS)*, 1993.
- Buciluă, C., Caruana, R., and Niculescu-Mizil, A. Model compression. In *Proceedings of the 12th ACM SIGKDD international conference on Knowledge discovery and data mining*, 2006.
- Caron, M., Touvron, H., Misra, I., Jégou, H., Mairal, J., Bojanowski, P., and Joulin, A. Emerging properties in self-supervised vision transformers. In *Proceedings of the IEEE/CVF international conference on computer vision*, 2021.
- Chen, S., Wu, Y., Wang, C., Liu, S., Tompkins, D., Chen, Z., Che, W., Yu, X., and Wei, F. Beats: Audio pre-training with acoustic tokenizers. In *International Conference on Machine Learning (ICML)*, 2023.
- Chen, T., Kornblith, S., Norouzi, M., and Hinton, G. A simple framework for contrastive learning of visual representations. In *International conference on machine learning (ICML)*, 2020.
- Chen, W., Liang, Y., Ma, Z., Zheng, Z., and Chen, X. Eat: Self-supervised pre-training with efficient audio transformer. In *International Joint Conference on Artificial Intelligence (IJCAI)*, 2024.
- Chen, X. and He, K. Exploring simple siamese representation learning. In *IEEE/CVF Conference on Computer Vision and Pattern Recognition (CVPR)*, 2020.
- Darcet, T., Baldassarre, F., Oquab, M., Mairal, J., and Bojanowski, P. Cluster and Predict Latent Patches for Improved Masked Image Modeling. *TMLR*, 2025.
- Devlin, J., Chang, M.-W., Lee, K., and Toutanova, K. Bert: Pre-training of deep bidirectional transformers for language understanding. In *Proceedings of the North American Chapter of the Association for Computational Linguistics (NAACL)*, 2019.
- Dosovitskiy, A., Beyer, L., Kolesnikov, A., Weissenborn, D., Zhai, X., Unterthiner, T., Dehghani, M., Minderer, M., Heigold, G., and Gelly, S. An image is worth 16x16 words: Transformers for image recognition at scale. In *International Conference on Learning Representations (ICLR)*, 2021.
- Ermolov, A., Siarohin, A., Sangineto, E., and Sebe, N. Whitenig for self-supervised representation learning. In *International Conference on Machine Learning (ICML)*, 2021.
- Evci, U., Dumoulin, V., Larochelle, H., and Mozer, M. C. Head2toe: Utilizing intermediate representations for better transfer learning. In *International Conference on Machine Learning (ICML)*, 2022.

- Gemmeke, J. F., Ellis, D. P. W., Freedman, D., Jansen, A., Lawrence, W., Moore, R. C., Plakal, M., and Ritter, M. Audio Set: An ontology and human-labeled dataset for audio events. In *IEEE International Conference on Acoustics, Speech and Signal Processing (ICASSP)*, 2017.
- Ghaffari, H. and Devos, P. On the role of audio frontends in bird species recognition. *Ecological Informatics*, 2024.
- Ghaffari, H. and Devos, P. Robust weakly supervised bird species detection via peak aggregation and pie. *IEEE Transactions on Audio, Speech and Language Processing*, 2025.
- Gong, Y., Lai, C.-I., Chung, Y.-A., and Glass, J. Ssast: Self-supervised audio spectrogram transformer. In *Proceedings of the AAAI Conference on Artificial Intelligence (AAAI)*, 2022.
- Grill, J.-B., Strub, F., Altché, F., Tallec, C., Richemond, P. H., Buchatskaya, E., Doersch, C., Pires, B. A., Guo, Z. D., Azar, M. G., Piot, B., Kavukcuoglu, K., Munos, R., and Valko, M. Bootstrap your own latent: A new approach to self-supervised learning. In *Advances in Neural Information Processing Systems (NeurIPS)*, 2025.
- Hagiwara, M., Hoffman, B., Liu, J.-Y., Cusimano, M., Effenberger, F., and Zacarian, K. BEANS: The Benchmark of Animal Sounds. In *IEEE International Conference on Acoustics, Speech and Signal Processing (ICASSP)*, 2023.
- Hameed, H. W., Nanfack, G., and Belilovsky, E. Not Only the Last-Layer Features for Spurious Correlations: All Layer Deep Feature Reweighting. *arXiv preprint arXiv:2409.14637*, 2024.
- He, K., Fan, H., Wu, Y., Xie, S., and Girshick, R. Momentum contrast for unsupervised visual representation learning. In *Proceedings of the IEEE/CVF conference on computer vision and pattern recognition*, 2020.
- He, K., Chen, X., Xie, S., Li, Y., Dollar, P., and Girshick, R. Masked autoencoders are scalable vision learners. In *IEEE/CVF Conference on Computer Vision and Pattern Recognition (CVPR)*, 2022.
- Hinton, G., Vinyals, O., and Dean, J. Distilling the knowledge in a neural network. *arXiv preprint arXiv:1503.02531*, 2015.
- Huang, P.-Y., Xu, H., Li, J., Baevski, A., Auli, M., Galuba, W., Metze, F., and Feichtenhofer, C. Masked autoencoders that listen. In *Advances in Neural Information Processing Systems (NeurIPS)*, 2022.
- Kumar, A., Raghunathan, A., Jones, R., Ma, T., and Liang, P. Fine-tuning can distort pretrained features and underperform out-of-distribution. In *International Conference on Learning Representations (ICLR)*, 2022.
- Lee, Y., Chen, A. S., Tajwar, F., Kumar, A., Yao, H., Liang, P., and Finn, C. Surgical fine-tuning improves adaptation to distribution shifts. In *International Conference on Learning Representations (ICLR)*, 2023.
- Lillicrap, T. P., Hunt, J. J., Pritzel, A., Heess, N., Erez, T., Tassa, Y., Silver, D., and Wierstra, D. Continuous control with deep reinforcement learning. *arXiv preprint arXiv:1509.02971*, 2019.
- Niizumi, D., Takeuchi, D., Ohishi, Y., Harada, N., and Kashino, K. Byol for audio: Self-supervised learning for general-purpose audio representation. In *2021 International Joint Conference on Neural Networks (IJCNN)*, 2021.
- Niizumi, D., Takeuchi, D., Ohishi, Y., Harada, N., and Kashino, K. Masked spectrogram modeling using masked autoencoders for learning general-purpose audio representation. *arXiv:2204.12260*, 2022.
- Quab, M., Dariseti, T., Moutakanni, T., Vo, H., Szafraniec, M., Khalidov, V., Fernandez, P., et al. Dinov2: Learning robust visual features without supervision. *Transactions on Machine Learning Research (TMLR)*, 2024.
- Ott, M., Edunov, S., Baevski, A., Fan, A., Gross, S., Ng, N., Grangier, D., and Auli, M. fairseq: A fast, extensible toolkit for sequence modeling. *arXiv:1904.01038*, 2019.
- Peng, Z., Dong, L., Bao, H., Ye, Q., and Wei, F. Beit v2: Masked image modeling with vector-quantized visual tokenizers. *arXiv preprint arXiv:2208.06366*, 2022.
- Picak, K. J. Esc: Dataset for environmental sound classification. In *ACM International Conference on Multimedia (MM)*, 2015.
- Przewiżlikowski, M., Balestiero, R., Jasiński, W., Śmieja, M., and Zieliński, B. Beyond [CLS]: Exploring the true potential of masked image modeling representations. *arXiv preprint arXiv:2412.03215*, 2025.
- Psomas, B., Christopoulos, D., Baltzi, E., Kakogeorgiou, I., Aravanis, T., Komodakis, N., Karantzalos, K., Avrithis, Y., and Tolias, G. Attention, please! revisiting attentive probing for masked image modeling. *arXiv:2506.10178*, 2025.
- Qiu, Z., Wang, Z., Zheng, B., Huang, Z., Wen, K., Yang, S., Men, R., Yu, L., Huang, F., Huang, S., Liu, D., Zhou, J., and Lin, J. Gated attention for large language models: Non-linearity, sparsity, and attention-sink-free.

- In *Advances in Neural Information Processing Systems (NeurIPS)*, 2025.
- Rauch, L., Heinrich, R., Ghaffari, H., Miklautz, L., Moummad, I., Sick, B., and Scholz, C. Unmute the patch tokens: Rethinking probing in multi-label audio classification. *arXiv:2509.24901*, 2025a.
- Rauch, L., Heinrich, R., Moummad, I., Joly, A., Sick, B., and Scholz, C. Can masked autoencoders also listen to birds? *Transactions on Machine Learning Research (TMLR)*, 2025b.
- Rauch, L., Schwinger, R., Wirth, M., Heinrich, R., Huseljic, D., Herde, M., Lange, J., Kahl, S., Sick, B., Tomforde, S., and Scholz, C. BirdSet: A Large-Scale Dataset for Audio Classification in Avian Bioacoustics. In *International Conference on Learning Representations (ICLR)*, 2025c.
- Tarvainen, A. and Valpola, H. Mean teachers are better role models: Weight-averaged consistency targets improve semi-supervised deep learning results. In *Advances in Neural Information Processing Systems (NeurIPS)*, 2017.
- Tu, C.-H., Mai, Z., and Chao, W.-L. Visual Query Tuning: Towards Effective Usage of Intermediate Representations for Parameter and Memory Efficient Transfer Learning. In *IEEE/CVF Conference on Computer Vision and Pattern Recognition (CVPR)*, 2023.
- Turian, J., Shier, J., Khan, H. R., Raj, B., Schuller, B. W., Steinmetz, C. J., Malloy, C., Tzanetakis, G., Velarde, G., McNally, K., Henry, M., Pinto, N., Noufi, C., Clough, C., Herremans, D., Fonseca, E., Engel, J., Salamon, J., Esling, P., Manocha, P., Watanabe, S., Jin, Z., and Bisk, Y. Hear: Holistic evaluation of audio representations. *arXiv:2203.03022*, 2022.
- Warden, P. Speech Commands: A Dataset for Limited-Vocabulary Speech Recognition. *arXiv:1804.03209*, 2018.
- Xiao, G., Tian, Y., Chen, B., Han, S., and Lewis, M. Efficient streaming language models with attention sinks. In *International Conference on Learning Representations (ICLR)*, 2024.
- Yang, S.-W., Chi, P.-H., Chuang, Y.-S., Lai, C.-I. J., Lakhotia, K., Lin, Y. Y., Liu, A. T., Shi, J., Chang, X., Lin, G.-T., Huang, T.-H., Tseng, W.-C., tik Lee, K., Liu, D.-R., Huang, Z., Dong, S., Li, S.-W., Watanabe, S., Mohamed, A., and yi Lee, H. Superb: Speech processing universal performance benchmark. In *Interspeech*, 2021.
- Zbontar, J., Jing, L., Misra, I., LeCun, Y., and Deny, S. Barlow twins: Self-supervised learning via redundancy reduction. In *International Conference on Machine Learning (ICML)*, 2021.
- Zhang, J. O., Sax, A., Zamir, A., Guibas, L., and Malik, J. Side-Tuning: A Baseline for Network Adaptation via Additive Side Networks. In *European Conference on Computer Vision (ECCV)*, 2020.
- Zhou, J., Wei, C., Wang, H., Shen, W., Xie, C., Yuille, A., and Kong, T. ibot: Image bert pre-training with online tokenizer. In *International Conference on Learning Representations (ICLR)*, 2022.

A. Hyperparameters

Table 6. Hyperparameter configurations. We show our hyperparameters for pre-training, fine-tuning, CGP, and linear probing.

Hyperparameters	Pre-Training AS-2M	Fine-Tuning				CGP/Linear Probing					
		AS-2M	AS-20K	ESC-50	SPC-2	AS-2M	AS-20K	ESC-50	SPC-2		
Optimizer		AdamW									
Optimizer Momentum		$\beta_1 = 0.9, \beta_2 = 0.95$						$\beta_1 = 0.9, \beta_2 = 0.999$			
Weight Decay	0.05	0.05						0.5/0.005			
Learning Rate Schedule		Cosine									
Peak Learning Rate	5e-4	5e-5	5e-5	5e-5	5e-5	1e-6	1e-3				
Minimum Learning Rate											
Steps	400K	400K	40K	4K	40K	200K	20K	4K	40K		
Warm-up steps	53K	40K	4K	400	4K	2K	2K	400	4K		
Batch size	12	96	48	48	256	96	48	48	256		
Clone Views	16	N/A									
GPUs	4	1									
Drop path	0.0	0.1	0.1	0.1	0.1						
Weighted Sampling	False	True	False	False	False						
Weighted Sampling size	N/A	200K	N/A	N/A	N/A						
Noise Augmentation	False	False	False	False	True						
SpecAug	N/A	0.2	0.2	0.2	0.1						
Mixup	0.0	0.9	0.9	0.0	0.9						
Layer-Wise LR Decay	N/A	0.75	0.75	0.75	0.75						
Loss Function	MSE	BCE	BCE	CE	BCE	BCE	BCE	CE	BCE		
Prototypes		N/A						10,000/0			

B. Resources

Most of the experiments were computed on NVIDIA A100 GPUs. This includes the multi-GPU SSL runs for pre-training and the downstream probes and fine-tuning. Smaller tests and code development were done on a workstation using an NVIDIA RTX4090 GPU and an AMD Ryzen 9 7950X CPU.

C. Datasets

In related audio SSL works that chase state-of-the-art (SOTA) on AudioSet, the mainly used datasets are: AS-2M, AS-20k, ESC-50, and Speech Commands V2. The pre-training is done solely on AS-2M. [Table 7](#) provides an overview of these datasets

[Table 7. Overview datasets.](#)

Dataset	Train	Validation	Test	#Classes	Segments [s]
<i>Multi-label</i>					
AS-2M	1,932,574	-	18,886	527	10
AS-20k	20,550	-	18,886	527	10
<i>Multi-class</i>					
esc50	1,600	-	400	50	5
sc2	84,848	9,982	4,890	12	10

D. Additional Results

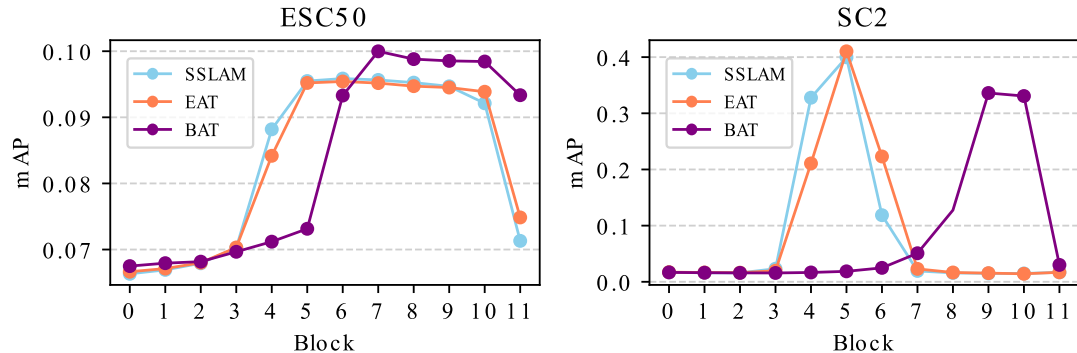


Figure 6. CGP weights for multi-class datasets. The weights are comparable to AS-20k weights we show in the main paper. We see that BAT shifts the information more towards the final layers.